Tuijin Jishu/Journal of Propulsion Technology
ISSN: 1001-4055
Vol. 45 No. 1 (2024)

Modelling and Simulation of HS-IMPATT Devices based on Graphene/SiC for D-band Applications

[1]Mamata Rani Swain*, [2]Pravash Ranjan Tripathy
[1]Department of Electronics & Communication Engg.
Biju Patnaik University of Technology, Odisha, India
[2]Department of Electronics and Communication Engineering
Gandhi Engineering College Odisha, India

Abstract: - A numerical simulation of a Hetero-structure based Graphene/4H-SiC and Homo-structure based Graphene, 4H-SiC double-drift region (DDR) impact ionization avalanche transit time (IMPATT) diodes operating at 140Gz is presented in this paper. By using drift-diffusion model the authors investigated the DC, small-signal properties of IMPATT diodes. The comprehensive simulation results show that, in comparison to its other counterparts, the Graphene/4H-SiC DDR IMPATT performs better in terms of efficiency and output power. With an ideal bias current density of $6.51\times10^{8}A/m^{2}$, the Graphene/4H-SiC DDR IMPATT diode yields a conversion efficiency of 18.4% and and an output power of 38.73W, respectively, demonstrating its superiority over other IMPATTs. The design findings in this work are highly promising and useful in the realization of these diodes for millimeter-wave communication systems

Keywords*: Graphene, Heterostructure, silicon carbide (SiC), double-drift region (DDR), IMPATT.*

1. Introduction

IMPATT diodes are solid state devices that can provide a high power at both microwave and millimeter-wave frequency bands [1]. The reported frequencies of operation and the output power obtained from IMPATT oscillators from the date of first experimental report show continuous improvement in subsequent years. The output power generation of the order of 100W in X, about a watt in W-band for IMPATT diodes is a good achievement [2]. A pulsed power of 42W at 96GHz [3], CW power of 980mW at 100GHz, 50mW at 220GHz [4] are significant report as far as IMPATT performance is concerned. The improvement of fabrication [5] and advancement of device technology led to the development of IMPATT diodes with modulated doping profiles and the realization of hetero-junction [6] and hetero-structure [7] IMPATT diodes. These factors have led the IMPATT based devices to be premier solid state devices for microwave generation. In recent years, several researchers have reported [8] [9] [10] the wide band-gap materials (GaN, SiC) as the base material of IMPATT diodes for generation of high power. However, numerous studies emphasized in the simulation and fabrication of heterostructure IMPATT diodes. Subsequently, an increasing number of studies focused on the modeling and simulation of heterostructures [11] [12] [13] like GaAs/Ge, P-GaN/n-SiC and Si/SiC goals to obtain low noise, high RF output power, and high DC-to-RF conversion efficiency. With the advancement of device technology, new materials are explored to improve the performance of IMPATTs at high frequency.

The semiconductor industry is putting more focus on new materials and devices that could make devices work better or give them new functions. Recent research has shown that Graphene as one of the thinnest and strongest material (in the nm range) in the universe whose charge carrier exhibits giant intrinsic mobility [14]. Graphene is becoming the next-generation electronic material due to its single atomic layer that is zero-band gap and excellent electronic properties, like high electrical conductivity, high electron mobility, and tenability [15]. The performance of graphene-based heat sink for double-drift region IMPATT structure is presented [16]. Owing to interesting and considerable electronic properties of graphene, a double drift region (DDR) IMPATT is proposed based on

graphene-silicon carbide (SiC) substrate [17]. A parallel connected GNR-based IMPATT structure is proposed [18] with power-combining capability in millimeter-wave and terahertz frequencies and studied the static, high-frequency, and noise performance. This report [19] revealed the computational effect of the transverse magnetic fields on the performance of graphene -based Impact Avalanche Transit Time (IMPATT) diodes
The found results above mentioned encouraged the authors to explore the Graphene/4H-SiC heterostructure. This paper examines the comparative performance of the homostructure based Graphene, 4H-SiC and the DDR Graphene/4H-SiC based heterostructure IMPATT diode at 140 GHz window frequency. The optimum bias current density is used to compare the DC and radio frequency performance of the devices, considering the effect of space charge, which provides the necessary information on design parameters for the future realization of these devices.

2. Simulation Models and Methods

In this simulation, the one-dimensional (1-D) DDR-based IMPATT (n+-n-p-p+) diode shown in fig.1 is studied. The IMPATT device works because the frequency of the charge carriers depends on how long it takes for them to move the transit time(τ_T). The author first set up the IMPATT for a certain design frequency (fd) using the empirical formula $w_{n,\,p} = 0.37\, v_{sn,\,sp}/f_d$ [20] where v_{sn}, v_{sp} are the electron and hole drift speeds at saturation, and w_n and w_p are the widths of the n-side and p-side depletion areas. As a result, the depletion layer decreases with an increase in operating frequency. Depletion width decreases, resulting in an increase in charge density. The electric field increases with operating frequency because it is related to the integral of charge density. The exact electric field profile and carrier current profile in the depletion layer are necessary to analyze the DC properties of the IMPATT diode The models do not take into account the widths of the n+ and p+ zones, despite the fact that these regions contain a significant amount of doping. The background doping concentrations of n- and p- layers are initially chosen in order of $10^{23} m^{-3}$according to the design frequencies.

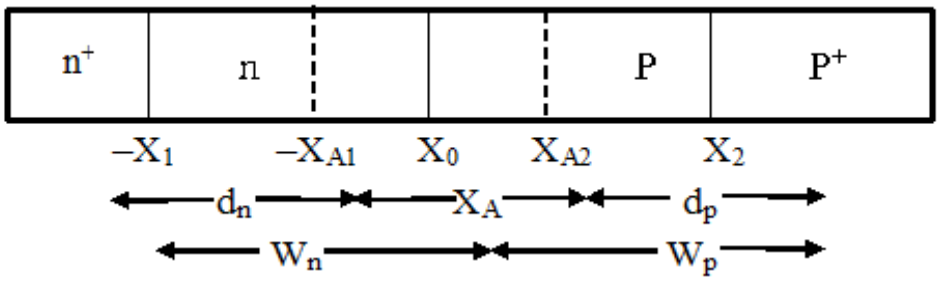

(a)Homo-structure

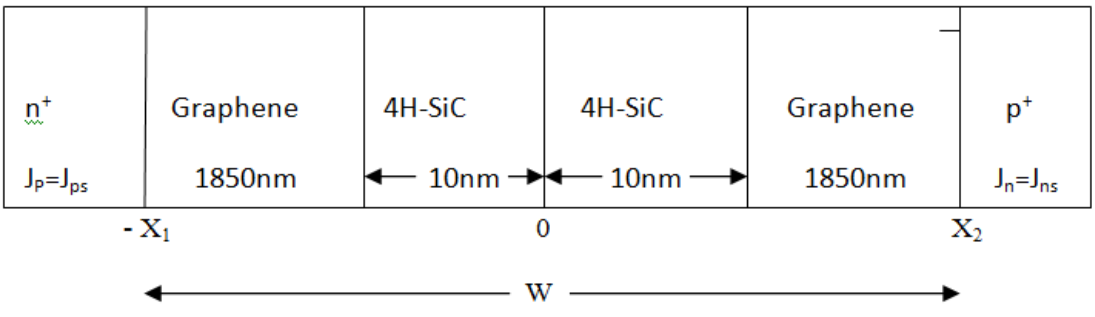

(b) Hetero-structure

Figure 1. Schematic Diagram of Double Drift base (a)Homo-structure and (b) Hetero-structure IMPATT Diode at 140 GHz

In this paper, the author has collected the recently reported values of material parameters, which are listed in Table 1 [19] [21] [22]. The design parameters based on these materials are enclosed in Table 2 at the 140 GHz design frequency. To study the complete RF performance of the DDR IMPATT diode, it is necessary to perform DC simulation followed by small-signal simulation. The structural and doping parameters, design frequency, all material parameters, and bias current density are entered as inputs for the simulation process.

Table 1. Graphene and 4H-SiC in terms of their material parameters

Parameters	Graphene	4H-SiC
Band gap energy Eg (ev)	< 0.3	3.26
Hole saturation velocity, $v_{sp}(10^5 m/s)$	6.9	1.08
Electron saturation velocity $v_{sn}(10^5 m/s$	7.0	2.12
Mobility of electrons , μ_n $(m^2v^{-1}s^{-1})$	25	0.1
Mobility of holes , μ_p $(m^2v^{-1}s^{-1})$	23	0.01
Permittivity ,ε $(10^{-11}Fm^{-1})$	8.856	9.66

Table 2. Design parameters DDR IMATT diodes at 140 GHz

Materials	f_d (GHz)	N_D $(\times10^{23}m^{-3})$	N_A $(\times10^{23}m^{-3})$	J_0 $(\times10^8 Am^{-2})$	W_n (nm)	W_P (nm)	W (nm)	D_j (μm)
Graphene	140	7.00	6.13	1.31	1850	1850	3700	25
4H-SiC	140	4.90	5.00	9.00	400	400	800	25
Graphene/4H-SiC	140	4.30	4.18	6.51	1860	1860	3720	25

2.1 DC simulation

The computer simulation method initiates with DC analysis, which is described in greater detail elsewhere [23] [24] [25]. To start the computation, the value of the field maximum E_0 and its location x_0 are suitably chosen for the diode. Thus, the DC field profile and carrier current distribution profile for a particular IMPATT diode operating at a given current density are obtained from the final solution of E_0 and x_0. A computer algorithm has been created to solve Poission's equation, carrier continuity equations, and the space charge equation simultaneously. The electric and carrier current profiles can be obtained by taking into account the effects of mobile space charge and carrier diffusion. The method described above gives the avalanche breakdown characteristics of the IMPATT diode. The voltage drops across different zones, i.e., avalanche voltage drops (V_A) and breakdown voltage (V_B), is determined by integrating the electric field over the respective width of the total depletion layer. By integrating the field profile over the total depletion layer width, the breakdown voltage is calculated and given by

$$V_B = \int_{-X_1}^{X_2} E(x)d(x) \tag{1}$$

Here x_1 and x_2 are width of n-side and p-side depletion layer

DC to RF conversation efficiency [24] defined as

$$\eta(\%) = \frac{2mV_D}{\pi V_B} \tag{2}$$

Here, V_D (V_B- V_A) is the voltage drop across the drift region.

2.2. Small signal simulation

The high-frequency analysis of the drift IMPATT diode reveals its high-frequency performance. When the ac field in the depletion region is very small compared to the dc breakdown field, the variation of the ionization rate

with the electric field can be assumed to be a linear and small-signal solution of time-varying Poisson's, and continuity equations can be carried out for linearization, which represents the amplitude limit of large-signal analysis. Gummel and Blue [26] presented a small-signal analysis of the basic equations that was free from simplifying assumptions about carrier properties. The Gummel-Blue approach is a simple way to calculate the negative conductance of the diode for a range of frequencies. From the DC electric field profile and current profile, the carrier ionization rates that appear in the Gummel-Blue equations are evaluated and fed as input data for the small signal analysis. The small signal parameters, such as negative conductance (-G), susceptance (B), impedance (Z), and bandwidth of the diode, satisfy the boundary condition [26].

Total integrated negative resistance (Z_R) and reactance (Z_X) of diodes at a specific frequency (ω) can be calculated by numerically integrating the resistivity (R) and reactivity (X) profiles over the depletion layer width (w) as follows:

$$Z_R = \int_0^w R dx \tag{3}$$

$$Z_X = \int_0^w X dx \tag{4}$$

Diode impedance is given as $Z(x,\omega) = R(x,\omega) + jX(x,\omega)$ (5)

The total impedance is given by $Z_{Total} = \int_0^w Z(x,\omega) dx = Z_R + jZ_X$ (6)

The negative conductance and susceptance is calculated as

$$-G = \frac{-Z_R}{\left[(Z_R)^2 + (Z_X)^2\right]} \tag{7}$$

$$B = \frac{Z_X}{\left[(Z_R)^2 + (Z_X)^2\right]} \tag{8}$$

The small signal quality factor (Q_p) is calculated as

$$-Q_P = \frac{B_P}{G_P} \tag{9}$$

The analysis of small signal is repeated for various frequencies. The frequency at which the negative conductance ($-G_P$) reaches its peak position is known as the optimal frequency (f_P). From this analysis, the diode negative resistance ($-Z_R$) and the reactance (Z_X) can also be determined at the optimal frequency (f_P). At a given current density, f_P is the peak frequency at which the negative conductance is maximum and the quality factor is minimum. Then the RF power obtained from the IMPATT can be calculated as [26]

$$P_{RF} = (V_{RF})^2 |G_P| \times -\frac{A}{2} \tag{10}$$

Where V_{RF} is the RF voltage, $V_{RF} = m_x \times V_B$, (11)

Where m_x equals 50% of modulation, $|G_P|$ is the peak magnitude of the negative conductance at the peak optimum frequency (f_p), where A ($\pi(D_j/2)^2$) is the area of the diode

Table 3. DC and Small signal parameters of DDR IMPATT Diodes at 140 GHz

Structures / parameter	Graphene	4H-SiC [27]	Graphene/4H-SiC
Design frequency(fd)	140	140	140
Em(10^8V/m)	0.480	3.8	4.02
breakdown voltage ,V_B(V)	37.4	158.19	184.13
Negative conductance,G_P(10^7Sm^{-2})	0.9834	4.21	1.863
Susceptance,B_P(10^7Sm^{-2})	1.096	1.3511	5.931
Efficiency, η(%)	10.8	15.77	18.4
Optimal frequency (f_p)	145	140	145
RF power (W)	0.822	15.9	38.73
Quality factor (Q)	1.12	0.32	3.18

3. Results and Discussion

The results obtained from the DC analysis of the IMPATT diode are described in this section.The method used here is as described in Chapter 2. Here, the graphene/4H-SiC heterodiode structure arranged by n-Graphene-4H-SiC/P-4-H-SiC-Graphene has been designed at 140 GHz. The peak electric field, breakdown voltage, efficiency, and avalanche zone widthcalculated for this structure are presented in Table 3. The efficiency of HS Graphene/4H-SiC is about 18.4% compared to that of 4H-SiC as it is 15.77% [27], and graphene, which is 10.8%.The electric field is high about 4.02×10^8 (V/m) as compared to its counterparts (3.8×10^8V/m) and (0.480×10^8V/m. The break-down voltage of HS graphene/4H-SiC is higher (184.13 V) than that of 4H-SiC homostructure (158.19) and graphene (37.4 V).

Figure 2 shows the relationship between negative conductance and frequency between differentIMPATT diodes, and it is observed that 4H-SiC DDR IMPATT diodes have a higher conductance of about $4.215\times10^7Sm^{-2}$ at 140 GHz frequency. Figure 3 shows the efficiency and RF power versus the current density for a graphene/4H-SiC DDR IMPATT HS diode. The figure shows that by increasing current density, efficiency decreases and RF power increases.

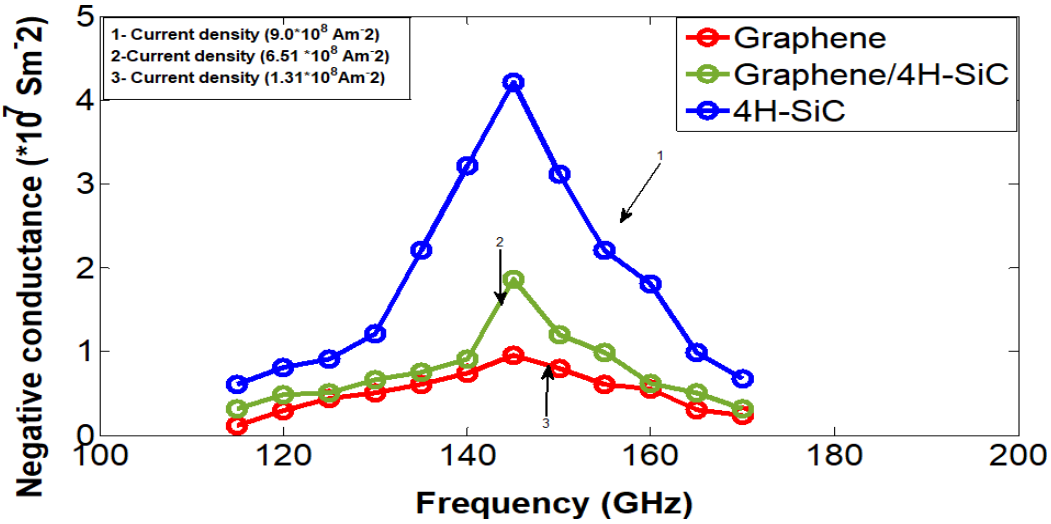

Figure 2. Plot between negative conductance and frequency of different diodes.

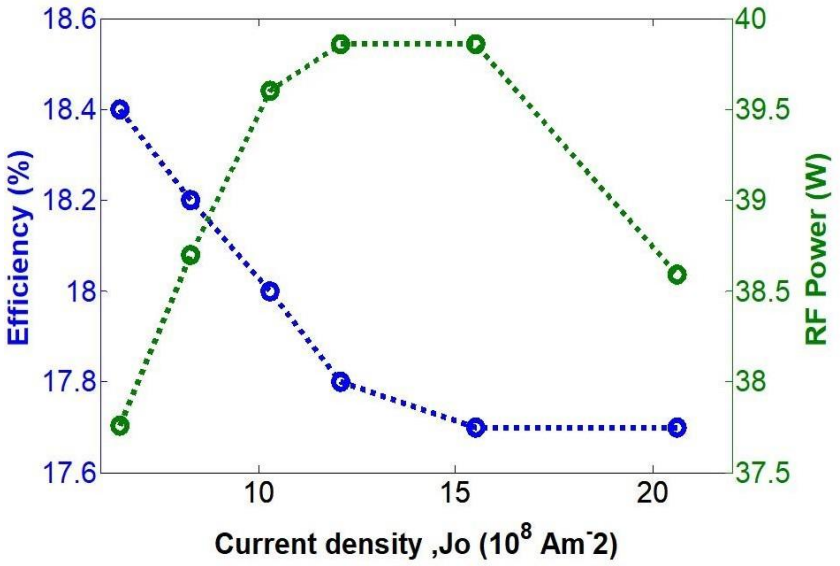

Figure 3. Plot the relationship between efficiency and RF power of Graphene/4H-SiC IMPATT diode current density at 140 GHz frequency.

Figure 4 shows The admittance characteristics of different DDR IMPATT diodes at 140 GHz.The HS Graphene/4H-SiC DDR IMPATT diode, the 4H-SiC DDR IMPATT diode, and the graphene diode all have similar admittance properties. The highest conductivity of HS DDR IMPATT is at a frequency of 145 GHz. The highest conductivity of 4H-SiC DDR IMPATT is at a frequency of 140 GHz, and the highest conductivity of graphene DDR is also at a frequency of 145 GHz. In Figure 5, figure out the IMPATT devices of the three structure's RF power and DC-RF conversion efficiency with respect to frequency. Based on the findings, the HS DDR IMPATT diode has more RF power, a wider frequency range, and a better ability to convert DC to RF. Because the HS DDR-IMPATT diode has a high DC breakdown voltage, it is possible to get higherRF voltages, which leads to more RF power and better efficiency.

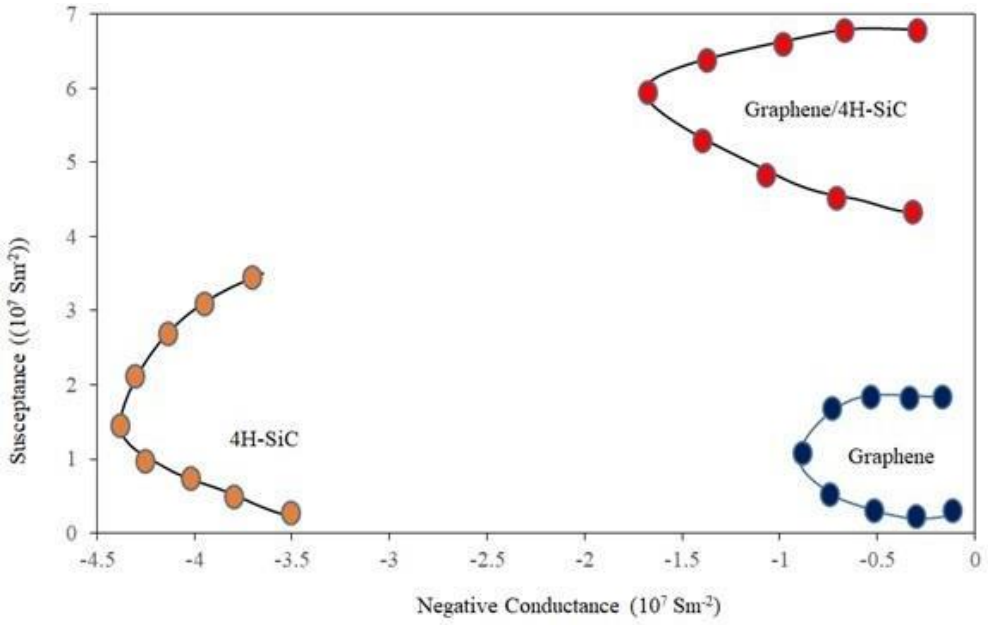

Figure 4. The admittance characteristics of different DDR IMPATT diodes at 140 GHz

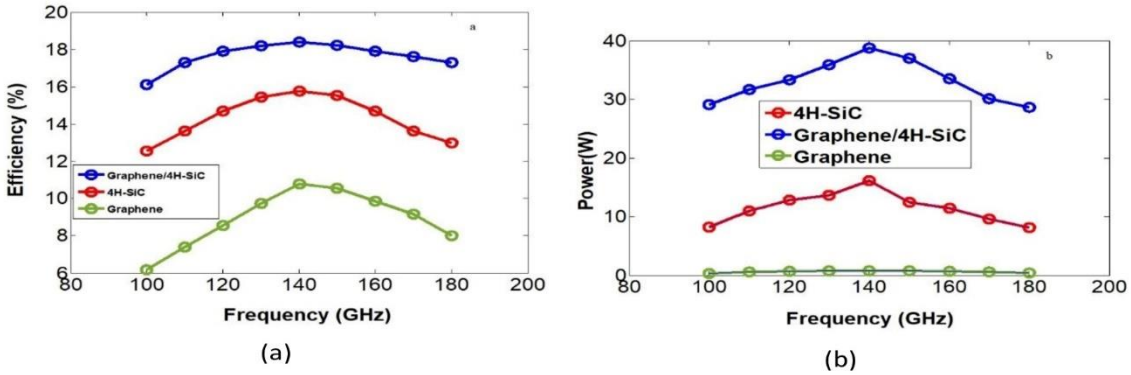

Figure 5. The relationship between (a) efficiency and (b) RF power versus frequency of different IMPATT diodes at 140 GHz

The HS DDR IMPATT diode works best at the peak frequency of 145 GHz. This is because the p-type drift region and the n-type drift region were designed to meet each other. At the best frequencyof 145 GHz, the HS DDR IMPATT diode has an RF power of 38.73 W and a DC-RF conversion efficiency of 18.4%, while the 4H-SiC DDR IMPATT has an RF power of 16.18 W and a DC-RF conversion efficiency of 15.77%. The RF output power of HS DDR IMPATTdiodes is much higher than that of 4H-SiC DDR IMPATT diodes, and the efficiency of converting DC to RF has also been increased to some degree.

The voltage modulation factor m of the DDR IMPATT device is controlled by varying the applied voltage to obtain the conductance, RF power, and efficiency as a function of frequency,as depicted in Figure 6. In the 100–180 GHz frequency band, as the modulation factor m increases, the conductance decreases while efficiency and RF power gradually increase. It indicates that the efficiency and RF power of the device can be increased near the optimal frequency by increasing the device's RF voltage.

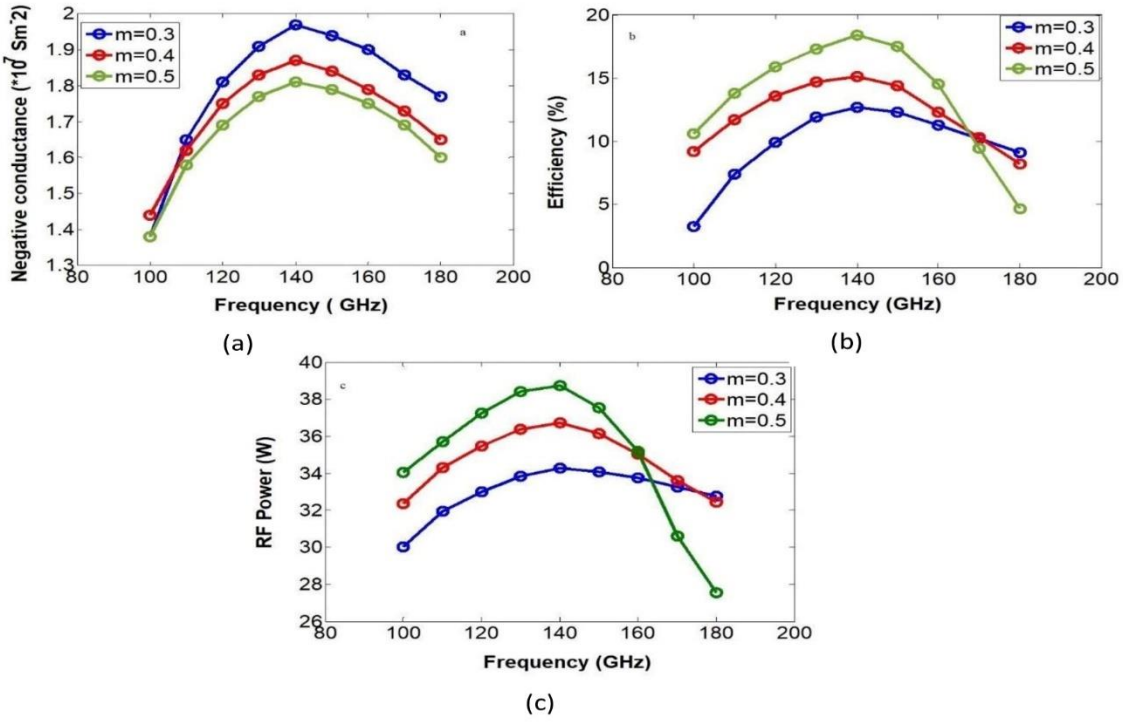

Figure 6. (a) Negative conductance, (b) Efficiency, and (c) RF Power of Graphene/4H-SiC IMPATT verses frequency with varying modulation factor m.

Figure 7 shows the RF power and efficiency for HS DDR IMPATT and 4H-SiC DDR IMPATTat 140 GHz as a function of the voltage modulation factor m. Both systems are changing in the same way. As m goes up, both the RF power and the efficiency go up at first, but once they hit the saturation value, they start to go down. When m is 0.55, the RF performance of HS- IMPATT is maximum, but when m is less than 0.3, the RF performance of 4H-SiC DDR IMPATT is maximum.

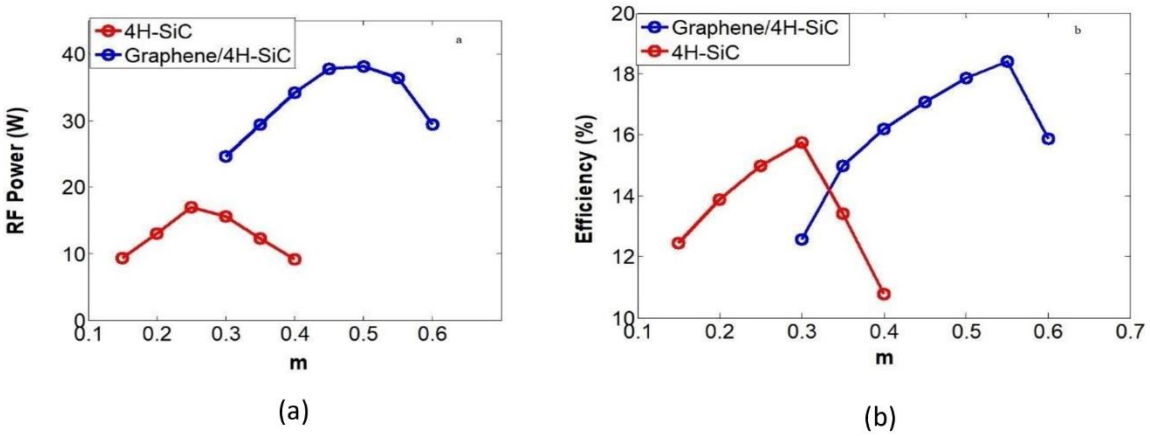

Figure 7. (a) power (w) and (b) Efficiency (%) with respect to voltage modulation factor m at 140 GHz

4. Conclusion

This study offers a heterojunction-based graphene/4H-SiC IMPATT diode that uses 4H-SiC instead of immature graphene to build DDR diodes and makes their design easier. The new structure has higher RF power and DC-RF conversion efficiency, according to the research. The graphene/4H-SiC DDR IMPATT diode suggested in this paper can get 38.73 W of RF power at 145 GHz with a fixed DC bias current density. This is a lot more than the homogeneous DDR-IMPATT diode can do under the same conditions. The effectiveness of converting DC to RF has also improved. Simulations show that the frequency bandwidth and RF voltage modulation factor m of the DDR IMPATT diode are both higher. So, it gives a newway to create and build IMPATT devices using semiconductor materials with a wide bandgap.

Reference:

[1] Midford, T. A., & Bernick, R. L. (1979). Millimeter-wave CW IMPATT diodes and oscillators. *IEEE Transactions on Microwave theory and Techniques*, *27*(5), 483-492.

[2] Hirachi, Y., Nakagami, T., Toyama, Y., & Fukukawa, Y. (1976). High-power 50-GHz double-drift-region IMPATT oscillators with improved bias circuits for eliminating low-frequency instabilities. *IEEE Transactions on Microwave Theory and Techniques*, *24*(11), 731-737.

[3] Behr, W., & Luy, J. F. (1990). High-power operation mode of pulsed IMPATT diodes. *IEEE electron device letters*, *11*(5), 206-208.

[4] Midford, T. A., & Bernick, R. L. (1979). Millimeter-wave CW IMPATT diodes and oscillators. *IEEE Transactions on Microwave theory and Techniques*, *27*(5), 483-492.

[5] D. H. Lee et al. “Ion-Implanted Complementary IMPTT diode for D-band”, IEEE Proceeding Letters, pp. 1295-1296 (1974)

[6] Namordi, M. R., Shaw, D. W., & Doerbeck, F. H. (1979). Ge/GaAs heterojunction IMPATT's. *IEEE Transactions on Electron Devices*, *26*(7), 1074-1080.

[7] Dash, G. N., & Pati, S. P. (1994). Computer-aided studies on the microwave characteristics of InP/GaInAs and GaAs/GaInAs heterostructure single-drift-region impact avalanche transit time diodes. *Journal of Physics D: Applied Physics*, *27*(8), 1719.

[8] Yuan, L., Cooper, J. A., Melloch, M. R., & Webb, K. J. (2001). Experimental demonstration of a silicon carbide IMPATT oscillator. *IEEE Electron Device Letters*, *22*(6), 266-268.

[9] Sengupta, J., Ghivela, G. C., Gajbhiye, A., & Mitra, M. (2016). Measurement of noise and efficiency of 4H-SiC IMPATT diode at Ka-band. *International Journal of Electronics Letters*, *4*(2), 134-140..

[10] Tripathy, P. R., Mukherjee, M., & Pati, S. P. (2012). MM-wave performance and avalanche noise estimation of hexagonal SiC and GaN IMPATTs for D-band applications. *International Journal of Microwave and Wireless Technologies*, *4*(4), 473-481..

[11] Tripathy, P. R., S. K. Choudhury, and S. P. Pati. "A new model of heterostructure GaAs/Ge IMPATT diode at W-band frequency." AIP Conference Proceedings. Vol. 1832. No. 1. AIP Publishing, 2017.

[12] Dai, Y., Ye, Q., Dang, J., Lu, Z., Zhang, W., Lei, X., ... & Zhao, W. (2021). Study of p-SiC/n-GaN hetero-structural double-drift region IMPATT diode. *Micromachines*, *12*(8), 919.

[13] Mukherjee, M., Tripathy, P. R., & Pati, S. P. (2015). Si/SiC-based DD hetero-structure IMPATTs as MM-wave power-source: a generalized large-signal analysis. *Journal of Semiconductors*, *36*(6), 064005.

[14] Geim, A. K. (2009). Graphene: status and prospects. *science*, *324*(5934), 1530-1534.

[15] Ghivela, G. C., & Sengupta, J. (2020). The promise of graphene: A survey of microwave devices based on graphene. *IEEE Microwave Magazine*, *21*(2), 48-65.

[16] Ghivela, G. C. (2023). Prospects of graphene-based heat sink and its computational thermal analysis in avalanche transit time devices. *Journal of Computational Electronics*, 1-8.

[17] Ghivela, G. C., & Sengupta, J. (2019). Modeling and computation of double drift region transit time diode performance based on graphene-SiC. *International Journal of Numerical Modelling: Electronic Networks, Devices and Fields*, *32*(5), e2601.

[18] Acharyya, A. (2019). 1.0–10.0 THz radiation from graphene nanoribbon based avalanche transit time sources. *physica status solidi (a)*, *216*(7), 1800730.

[19] Ghivela, G. C., & Sengupta, J. (2020). Numerical study of magnetic field effect on graphene based IMPATT source. *Superlattices and Microstructures*, *137*, 106365.

[20] Sze, S. M., & Ryder, R. M. (1971). Microwave avalanche diodes. *Proceedings of the IEEE*, *59*(8), 1140-1154.

[21] Ghivela, G. C., & Sengupta, J. (2021). Space charge studies in graphene based avalanche transit time devices. *Superlattices and Microstructures*, *155*, 106899.

[22] Mukhopadhyay, S. J., Ghivela, G. C., Sengupta, J., & Mitra, M. (2021). Prospects and potentiality of diamond-based DDR IMPATTs in THz regime. *International Journal of Electronics Letters*, *9*(1), 36-46.

[23] Ghivela, G. C., Sengupta, J., & Mitra, M. (2019). Ka band noise comparison for Si, Ge, GaAs, InP, WzGaN, 4H-SiC-based IMPATT diode. *International Journal of Electronics Letters*, *7*(1), 107-116.

[24] Ghivela, G. C., & Sengupta, J. (2019). Noise performance of avalanche transit-time devices in the presence of acoustic phonons. *Journal of Computational Electronics*, *18*, 222-230.

[25] Ghivela, G. C., Sengupta, J., & Mitra, M. (2019). Quantum corrected drift diffusion based noise model for impact avalanche and transit time diode. *Superlattices and Microstructures*, *128*, 402-407.

[26] Gummel, H. K., & Blue, J. L. (1967). A small-signal theory of avalanche noise in IMPATT diodes. *IEEE Transactions on Electron Devices*, *14*(9), 569-580.

[27] Acharyya, A., & Banerjee, J. P. (2014). Prospects of IMPATT devices based on wide bandgap semiconductors as potential terahertz sources. *Applied Nanoscience*, *4*, 1-14.

[28] Raparthi, M., Dodda, S. B., & Maruthi, S. (2023). Predictive Maintenance in IoT Devices using Time Series Analysis and Deep Learning. Dandao Xuebao/Journal of Ballistics, 35(3). https://doi.org/10.52783/dxjb.v35.113